Proceedings of FEDSM2007
5th Joint ASME / JSME Fluids Engineering Conference
July 30 – Aug. 2, 2007, San Diego, CA, USA

FEDSM2007-37578

INVESTIGATION OF FUNDAMENTAL TRANSPORT MECHANISM OF PRODUCT WATER FROM CATHODE CATALYST LAYER IN PEMFCs

J. P. Owejan[1], J. E. Owejan[1], T. W. Tighe[1], W. Gu[1], M. Mathias[1]

[1]General Motors Fuel Cell Activities, 10 Carriage Street, Honeoye Falls, NY 14472, jon.owejan@gm.com

ABSTRACT

Understanding how water produced in the cathode catalyst layer is removed during PEMFC operation can be critical for materials optimization and representative models. The present work combines in-situ and ex-situ experiments to determine the dominant water discharge mechanism when considering capillarity and vapor transport. Water flux of vapor driven by the thermal gradient in the cathode diffusion layer is shown to be sufficient to remove product water at high current densities with saturated gas in the gas delivery channels. The role of an intermediate microporous layer and its impact in vapor versus liquid transport is also considered. Through novel experimental techniques and capturing all key physical interactions it is concluded that vapor diffusion is the fundamental mechanism by which water is removed from the cathode catalyst layer.

INTRODUCTION

Proton exchange membrane fuel cell (PEMFC) technology is widely considered to be a viable alternative to internal combustion engine (ICE) energy conversion systems. PEMFC systems are versatile and highly energy efficient with no direct contribution to greenhouse gas pollution. The path to PEMFC commercialization is continuously accelerated by research-driven technological improvements and society's growing awareness of the ill effects of petroleum consumption.

An important area of PEMFC research is the transport of the water produced from the oxygen reduction reaction at the cathode electrode. Mass transfer to and from the cathode electrode represents a significant limitation to fuel cell operation. On one hand, water is needed to keep the proton-conducting membrane hydrated so that voltage loss due to potential drop through the membrane is minimized. On the other hand, too much water within the cathode electrode will impede oxygen transport to the catalyst sites and result in significant voltage loss. An efficient fuel cell stack design requires a comprehensive understanding of water transport throughout the cathode volume.

A typical PEMFC assembly cross-section is shown in Figure 1, where the design is symmetric about the membrane. Figure 1 also describes the nominal pore size of each component and its respective surface properties. Outside the membrane, the system must be porous so that gas transport to the platinum catalyst can occur. The porous catalyst layer is laminated to the membrane. This layer must be thin to assure a short transport length within and allow for high catalyst utilization. The additional porous layers are required for in-plane transport of reactant gas around the electron conducting lands of the flow distributor channels. The bulk material of this layer is carbon fiber paper. An additional microporous layer (MPL) must be applied between the catalyst layer and the carbon fiber paper (gas diffusion layer) for optimal PEMFC performance [1-3]. A thermal gradient exists from the cathode electrode to the gas channels as heat is generated in association with the oxygen reduction reaction.

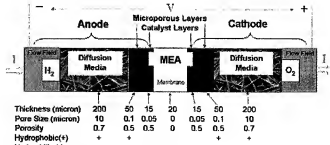

Figure 1 – Description of thickness and component pore size in a typical PEMFC cross section

Of particular interest in the current work and perhaps the most difficult to interrogate experimentally is the mechanism by which product water is transported away from the catalyst sites where it is produced. In this region of the fuel cell assembly (shown in Figure 1), transport occurs within the nano/micro pores indicated by the catalyst and microporous layers. The catalyst layer interface represents the smallest transport length scale in the system but is known to have the most significant impact on the overpotential associated with mass transfer [4-5]. For this reason it is imperative to determine the phase of water moving away from the cathode catalyst layer. Specifically, either the capillary driven transport associated with liquid water or diffusive transport associated with vapor needs to be identified as the dominant mechanism. The physics associated with the main mode of transport must be accurately captured for precise mass transport models. Moreover, this determination will allow for more astute material design.

There is a significant amount of published research focused on the development and application of diagnostic techniques to interrogate operating fuel cells for liquid water formation and dynamics [6-9]. In addition to these techniques, some claim to resolve the interface between the catalyst and gas diffusion layers with techniques such as Ramen spectroscopy, magnetic resonance imaging, neutron scattering, and neutron imaging [10-13]. The results from these experiments are found to be ambiguous with reference to the phase of water leaving the cathode catalyst layer, mainly due to limited spatial resolution.

Additional experiments regarding water transport from the catalyst layer are executed by evaluating the PEMFC polarization curve performance with various gas mixtures, flow-field geometry and interfacial material properties [14-16]. These referenced works generally agree with a vast body of PEMFC theoretical models that identify water in the liquid phase is removed from the electrode via capillary transport [17]. In order for the capillary transport mechanism to apply, an overall hydrophobic cathode electrode has to be assumed such that high pressure required to transport liquid water out of the electrode can be achieved without a complete flooding of the cathode electrode. However, this scenario is debatable because the electrode made of ionomer is hydrophilic in nature.

The current work introduces a series of novel *in-situ* and *ex-situ* experiments to further investigate water transport in this region of interest. These experiments unambiguously isolated vapor and liquid driven transport mechanisms and their relative importance on mass transport resistance. Water flux is accurately measured *ex-situ* for diffusion and pressure driven transport separately within the porous fuel cell components. The thermal gradient and hydraulic permeability of these components are then further exploited with *in-situ* experiments that confirm a physical model regarding water transport from the catalyst layer and actual role of the adjacent porous components.

EXPERIMENTAL

Ex-situ experiments were designed to first independently characterize pressure versus diffusion transport rates through the MPL (as shown in Figure 1). These rates are determined to verify that both mechanisms are capable of removing a flux of water equivalent to that produced in the PEMFC reaction. With these parameters characterized, *in-situ* experiments were executed using MPLs with and without large pore regions. Additional *in-situ* experiments manipulating the MPL location were designed to capture all elements of the transport theory.

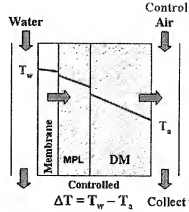

Figure 2 – Ex-situ thermal gradient experiment.

To determine the vapor diffusion rate through a MPL as a result of the naturally occurring temperature gradient in a PEMFC, an *ex-situ* experiment was developed. As described in Figure 2, a liquid water flow was provided adjacent to a water transferring membrane (Nafion® 111). The temperature of the water was well controlled and this temperature was used to simulate the temperature of the catalyst layer in an operating system. In the reported experiments the water temperature (T_w) was controlled at 80°C. The micro-porous layer (MPL) was positioned adjacent to the water saturated membrane opposite the liquid water supply. The MPL used for these experiments was a freestanding, crack-free 50 µm thick expanded PTFE layer that is impregnated with carbon black powder. This MPL has a similar mean pore size, hydrophobic surface, and thickness to the typical layers reported in PEMFC design [2]. The MPL was supported with a carbon fiber GDL (Toray® T060) and gas flow channel array. The assembly was compressed to 1.4 MPa with respect to the MPL area. The temperature of the flow field and incoming gas (T_a) was controlled independently of the water temperature allowing one to manipulate the temperature differential between the membrane and channel as it would occur in an operational PEMFC due to reaction waste heat. The system was verified to be hydraulically impermeable at the liquid pressure used in the experiment. With the amount of water entering the system known, the water exiting the system was condensed and measured. This allowed for the

determination of the vapor transfer rate for a give temperature differential and channel RH.

In this experiment (similar to an operating PEMFC), there are two factors driving vapor transport, channel RH and the induced temperature gradient within the diffusion layers. To determine the relative influence of each, the gas RH and the temperature differential were varied independently. The temperature differentials tested were 8, 4, and 0°C with both 50% and 100% RH channel flows.

To determine the hydraulic permeability of the MPL, a similar set-up as depicted in Figure 2 was employed but without a water transfer membrane. This allowed liquid water to hydraulically penetrate the MPL once a sufficient liquid water pressure was reached. In these experiments the liquid to air pressure differential was measured and recorded. As the water pressure was increased, eventually a breakthrough pressure was reached. This indicates the capillary pressure that would have to occur in the catalyst layer to sustain pressure driven transport.

With the liquid and vapor transport rates through the MPL confirmed to be sufficient, in-situ experiments were designed to demonstrate the effect of hydraulic permeability in the MPL. The gas diffusion layer (GDL), composed of a commercially available PTFE treated carbon fiber paper substrate that was coated with a micro-porous layer (MPL) consisting of carbon black powder and PTFE. Samples were produced such that one sample formed a continuous and crack free MPL coating, while the other sample was processed such that cracks formed in the final, dry coating. The micrographs shown in Figure 3 illustrate the large pores (in the form of cracks) created in the mud-cracked sample and the lack of cracks in the sample with a homogenous MPL.

These samples are contrasted by only the large (relative to mean pore size in MPL) mud cracks that were formed in one sample. This provides a discontinuity of capillary pressure gradient within the MPL without affecting other parameters. If resistance to pressure driven outflow of water in the liquid phase from the cathode catalyst layer impacts the mass transport, these samples will have drastically different performance. However, if outflow of water is in the vapor phase from the cathode catalyst layer to the cathode channel, these contrasting samples would have very little effect on performance. To make this distinction, in-situ 50 cm^2 experiments were conducted with the described samples configured as cathode GDL in separate tests. The reported results consist of polarization curves run in co-flow configuration at various conditions.

It is critical that the cracked and crack-free MPL samples have similar thermal properties. To confirm this, samples were characterized with ex-situ through plane thermal resistance testing. In this experiment the GDL is placed between two thermally conductive platens which are coated with a conductive paste. The sample is then compressed to 1.4 MPa. One side of the GDL is adjacent to the heat source while the other is adjacent to the heat sink; the flux is measured and the through plane thermal resistance is calculated. The thermal resistance was found to vary less than 2% for the cracked and crack-free samples.

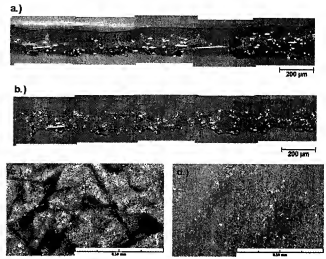

Figure 3 – SEM Micrographs of cross-sectioned cracked and crack-free MPLs a) continuous b) cracked, and optical microscopy of top down images c) cracked and d) continuous GDL samples.

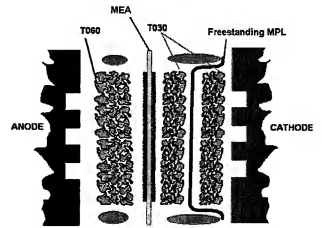

Figure 4 – Exploded view of cathode configurations with freestanding movable MPL (MPL in the center of cathode GDL shown)

A series of additional in-situ experiments were executed to further consider vapor versus (capillary pressure driven) liquid

transport from the cathode catalyst layer. These tests were designed particularly to determine where in the cathode diffusion layer liquid water limits mass transport of oxygen to the catalyst. This was characterized by moving the freestanding, crack-free MPL described above toward the cathode channel in various arrangements. These configurations were implemented by using two sheets of a thinner GDL substrate in the cathode. This thinner GDL substrate, Toray® T030, is roughly half the thickness of T060, which is utilized as the anode GDL. Both GDL substrates have similar surface properties, porosity, and permeability. The MPL was placed as described in Figure 4, in the center of the GDL. Additional configurations were also assembled in which i) the MPL was placed adjacent to the cathode channels, with the two pieces of T030 arranged adjacent to the cathode catalyst layer, ii) the MPL layer was omitted from the configuration altogether, and iii) where the MPL is placed in its traditional configuration: MPL adjacent to the catalyst layer with two pieces of T030 adjacent to the cathode channels.

RESULTS AND DISCUSSION

Vapor diffusion and capillary pressure driven transport mechanisms were first characterized with the ex-situ experiments previously described. The experimental variables for the vapor diffusion experiment (shown in Figure 2) were temperature differential through the GDL from the MPL interface to the flow distributor land interface and the relative humidity (RH) of the gas flowing through the flow distributor channels. The simulated temperature differential range is determined by the thermal bulk and contact resistance of the GDL with MPL combined with the heat loss associated with the difference between cell voltage and equilibrium voltage at a particular current density. A controlled differential temperature range from 0 to 8°C was selected for these experiments as it captures the expected temperature differential for a wide range of GDL thermal conductivity. The volumetric flow of air at a controlled RH was regulated at a high flow (5.0 slpm) such that the change in RH along the channel length was relatively small.

The results shown in Figure 5 are the water flux through the GDL by imposed temperature and water vapor concentration gradients. These data indicate that the measured rate is limited by the membrane material used. This is denoted by the relatively constant flux at all 50% RH temperature gradient test points. Since the vapor driving force is increased proportionally with temperature differential, one can conclude that the water source is rate limiting. For these experiments, the water flux that is transferred through Nafion® 111 is shown to be maximized at 0.01 g/s. Because the results indicate that the water flux is membrane limited, vapor transport through the MPL should be capable of accommodating this flux or higher.

Although the measured rate of vapor transfer is membrane limited, these results indicate that the flux of water driven by vapor diffusion is sufficient to remove the water produced in the cathode of a PEMFC operating at high current density. The 0% RH with 0°C temperature differential condition removes all driving force for water transfer, and small amount of water measured at this condition is used for experimental error estimation.

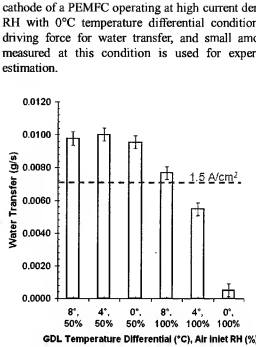

Figure 5 – Ex-situ diffusion driven transport at varying GDL temperature differentials and channel RH, flux associated with 1.5 A/cm² indicated by dashed line

Pressure driven capillary transport is also considered with the *ex-situ* experiments previously described. In these experiments the MPL side of the GDL is pressurized by applying a 1.0 A/cm² equivalent liquid water flow (15 mL/h). The differential pressure across the GDL indicates the capillary pressure that is required in the catalyst layer to drive capillary flow. In this experiment the break-through pressure is indicated by the maximum differential pressure. Results for MPL formulations with and without cracks are shown in Figure 6. These results reveal a drastic contrast in the liquid water pressure required to initiate flow through the MPL. The cracked MPL has a break-through pressure of 108 kPa as compared to the crack-free MPL will a break-through pressure greater than 200 kPa. The crack free MPL break-through pressure could not be reached with the current experimental apparatus. In fact, the capillary pressure equation (Equation 1) reveals that this break-through pressure could be near 1 MPa.

$$p_c = -\frac{4\sigma\cos\theta}{d} \qquad \text{Eq. 1}$$

Where σ = surface energy (72 dynes for water), θ = surface contact angle (140° for MPL), and d = pore diameter (0.2 μm in MPL)

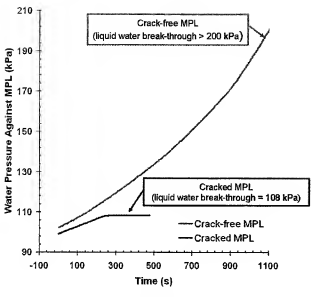

Figure 6 – MPL liquid water break-through pressure

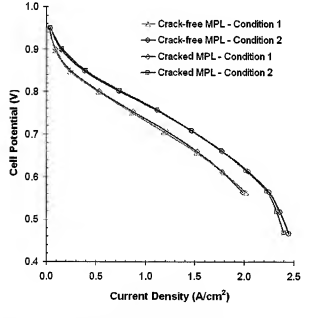

Figure 7 - Polarization Curve performance for crack and crack-free MPL samples

These results are compared with *in-situ* fuel cell experiments. The cracked and crack-free MPL samples are used as cathode GDLs in 50cm^2 cells. Condition 1 in Figure 7 is designed to operate with a slightly saturated cathode exhaust (110% estimated exhaust RH), specifically the test cell is controlled at 150 kPa, 66% inlet RH anode and cathode gas supply, 80°C cell temperature, and a 2/2 H_2/air stoichiomery. Condition 2 is intended to operate with high liquid water content (300% estimated exhaust RH), this is achieved by controlling at 270 kPa, 100% inlet RH anode and cathode gas supply, 60°C cell temperature and 2/2 H_2/air stoichiometry. These two conditions summarize a relatively humid environment typical to PEMFC application (condition 1) and a high liquid water environment for more immoderate mass transport diagnostics (condition 2). The polarization curve performance shown in Figure 7 summarizes the similar performance observed for the cracked and crack free samples at both operating conditions.

Results thus far indicate that vapor diffusion provides the primary mode of water transport from the cathode catalyst layer. The *ex-situ* vapor diffusion experiments showed that a sufficient flux can be supported while the *ex-situ* capillary pressure experiments indicated a drastic dependence on MPL cracks. Comparing these results with the nearly identical in-situ performance of cracked and crack-free MPLs indicates that product water is primarily removed in the vapor phase. If pressure driven liquid transport had a significant role, the high current density performance would be impacted by the crack-free MPL.

As noted previously, it is widely accepted that a MPL is required for optimal PEMFC performance. The fundamental mechanism for this improvement is often described with Darcy transport. The current work contradicts this by identifying vapor transport, a diffusive mechanism, as the primary mechanism that enables high current density PEMFC operation. To clarify and support this finding a new physical model must be considered as it is not immediately clear why an intermediate porous layer will aid diffusive transport.

The addition of a MPL in a PEMFC assembly reduces mass transport overpotenial by providing a barrier such that liquid water that condenses in the large pores of the GDL cannot make contact with the catalyst layer. Due to the temperature decrease through the thickness of the GDL, water vapor will condense near the flow field land interface where the mole fraction of water vapor exceeds saturation. This liquid water will fill portions of the porous GDL substrate but not the pores of the MPL as the capillary pressure required to do so is unachievable. The MPL primarily functions by providing an open structure for oxygen to diffuse around localized liquid water blockages in the GDL. Once the GDL pores reach a critical volume, liquid water is rejected into the gas delivery channels in the form of droplets that are subsequently removed by gas shear with the exhaust. Furthermore, the MPL provides an additional thermal resistance adjacent to the cathode catalyst layer, thus increasing the vapor pressure of product water. A schematic describing this functionality is shown in Figure 8.

Additional experiments were executed to verify the transport mechanism described in Figure 8. As previously described, the impact and location of condensation in the GDL was

characterized experimentally by moving the MPL incrementally from the cathode catalyst layer toward the cathode channels in separate experiments. As shown in Figure 9, the best performance is achieved with the MPL adjacent to the catalyst layer. As the MPL is moved to the center of the GDL and then to the channel interface the performance is shown to decrease. The relative performance loss without a MPL is also shown in Figure 9. The MPL used in these experiments increased mass transport loss when positioned away for the catalyst layer as condensed liquid water is trapped and allowed to contact the catalyst layer.

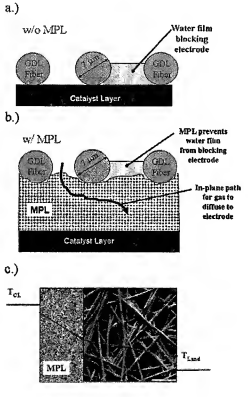

Figure 8 – Schematic of MPL function, a.) liquid water contacting catalyst layer without MPL, b.)diffusion around liquid water with GDL, c.) additional thermal resistance imposed by MPL.

When the MPL is against the cathode electrode it prevents condensed liquid water from contacting the catalyst. With the MPL removed, performance decreases as liquid water can back-up to the catalyst layer interface and the temperature differential through the thickness of GDL is decreased. Performance is further reduced with the MPL in the center of GDL as liquid water becomes trapped in the GDL because the break-through pressure into the MPL cannot be overcome. In the final experiment, where the MPL is at the channel interface,

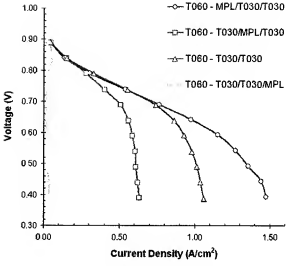

Figure 9 – Polarization curve performance of freestanding MPL cathode GDL configurations

mass transport losses dominate performance. This configuration has decreased performance when compared to the MPL in the center of the GDL configuration because the majority of condensed liquid water is near the channel interface were the system temperature is coolest. Thus, in this configuration more of the product water generated in the vapor phase is trapped before it can be transported into the flow field channels.

CONCLUSION

Novel in-situ and ex-situ experiments were developed and applied to PEMFC water management research. These experiments were focused on identifying the primary product water transport mechanism on the cathode side. The relative influence of liquid and vapor transport were isolated and considered independently. It is shown that thermal and vapor concentration gradients across the GDL are sufficient to remove product water at high current densities. It is also shown that capillary effects within the GDL have an insignificant effect on mass transport overpotential, thereby indicating Darcy flow in the cathode catalyst layer has little influence in the transport process.

The MPL improves PEMFC performance by providing a barrier that prevents condensed liquid water in the large pores of the GDL substrate from contacting the catalyst layer. With a MPL, an in-plane diffusion path around such liquid water blockages is provided. This functionality is confirmed by relocating the MPL in the cathode GDL, thus demonstrating the location of liquid water in the porous system and its lack of capillary driven transport at the electrode.

ACKNOWLEDGMENTS

Jason Thompson is acknowledged for his work with GDL temperature gradient and capillary pressure experiments. The authors would also like to thank Dr. Thomas Trabold for his critical review of this paper.

REFERENCES

1. M. Mathias, J. Roth, J. Fleming, W. Lehnert, Diffusion media for PEM fuel cells, Chapter 46 in: Handbook of Fuel Cells – Fundamentals, Technology and Applications, W. Vielstich et al. (Eds.), Volume 3: Fuel Cell Technology and Applications, John Wiley & Sons, Ltd. (2003).
2. Z. Qi, A. Kaufman, Improvement of water management by a microporous sublayer for PEM fuel cells, J. Power Sources **109** 38-46 (2002).
3. J. H. Nam, M. Kaviany, Effective diffusivity and water-saturation distribution in single and two-layer PEMFC diffusion medium, Int. J. of Heat and Mass Trans. **46** 4595-4611 (2003).
4. S. Listler, G. McLean, PEM fuel cell electrodes, J. Power Sources **130** 61-76 (2004).
5. I. E. Baranov, S. A. Grigoriev, D. Ylitalo, V. N. Fateev, I. I. Nikolaev, Transfer processes in PEM fuel cell: Influence of electrode structure, Int J. of Hydrogen Energy **31** 203-210 (2006).
6. K. Tuber, D. Pocza, C. Hebling, Visualization of water buildup in the cathode of a transparent PEM fuel cell, *J. Power Sources* **124** 403-414 (2003).
7. Q. Dong, J. Kull, M. M. Mench, Real-time water distribution in a polymer electrolyte fuel cell, *J. Power Sources* **139** 106-114 (2005).
8. J. Stumper, M. Lohr, S Hamada, Diagnostic tools for liquid water in PEM fuel cells, *J. Power Sources* **143** 150-157 (2003).
9. W. He, G. Lin, T.V. Nguyen, Diagnostic tool to detect electrode flooding in proton-exchange-membrane fuel cells, *AIChE J.* **49**, 3221-3228 (2003).
10. H. Matric, A. Lundblad, G. Lindbergh, P. Jacobsson, In-situ micro-Ramen on the membrane in a working PEM cell, Electrochem. and Solid-State Let. **8** (1) A5-A7 (2005).
11. R. Mosdale, G. Gebel, M. Pineri, Water profile determination in a running proton exchange membrane fuel cell using small-angle neutron scattering, J. of Membrane Science **118** 269-277 (1996).
12. S. Tsushima, K. Teranishi, K. Nishida, S. Hirai, Water content distribution in a polymer electrolyte membrane fuel for advanced fuel cell system with liquid water supply, Magnetic Resonance Imaging **23** 255-258 (2005).
13. R. J. Bellows, M. Y. Lin, M. Arif, A. K. Thompson, D. Jacobson, Neutron imaging technique for in-situ measurement of water transport gradients within Nafion in polymer electrolyte fuel cells, J. Electrochem. Soc. **146** 1099-1103 (1999).
14. U. Beuscher, Experimental method to determine the mass transport resistance of a polymer electrolyte fuel cell, J. Electrochem. Soc **153** A1788-A1793 (2006).
15. W. He, G. Lin, T. V. Nguyen, Diagnostic tool to detect electrode flooding in proton-exchange-membrane fuel cells, AIChE Journal **49** 3221-3228 (2003).
16. G. Lin, T. V. Nguyen, Effect of thickness and hydrophobic polymer content of the gas diffusion layer on electrode flooding level in a PEMFC, J. Electrochem. Soc. **152** A1942-A1948 (2005).
17. U. Pasaogullari, C. Y. Wang, Two-phase transport and the role of micro-porous layer in polymer electrolyte fuel cells, Electrochimica Acta **49** 4359-4369 (2004).